Lossless backward second-harmonic generation of extremely narrow subdiffractive beams in two-dimensional photonic crystals

C. Nistor,[1,*] C. Cojocaru,[1] T. J. Karle,[2] F. Raineri,[2,3] J. Trull,[1] R. Raj,[2] and K. Staliunas[1,4]

[1]*Universitat Politècnica de Catalunya, Departament de Física i Enginyeria Nuclear, Colom 11, E-08222 Terrassa, Spain*

[2]*Laboratoire de Photonique et de Nanostructures, Route de Nozay, F-91460 Marcoussis, France*

[3]*Université Paris Diderot, Paris, France*

[4]*Institució Catalana de Reserca i Estudis Avançats (ICREA), Barcelona, Spain*

(Received 10 June 2010; published 8 September 2010)

We report efficient second harmonic generation using extremely narrow beams (with diameter of the order of the wavelength) that propagate in the self-collimation (or nondiffractive) regime in a two-dimensional photonic crystal. We design and numerically test an AlGaAs photonic crystal membrane, where both fundamental and generated second harmonic beams propagate without diffraction and without out-of-plane losses. The characteristics of the generated second harmonic that is mainly propagating in the backward direction and the conversion efficiency of the proposed scheme are obtained by nonlinear finite-difference time-domain numerical simulations.

DOI: 10.1103/PhysRevA.82.033805 PACS number(s): 42.65.Ky, 42.70.Qs

I. INTRODUCTION

During the last two decades, photonic crystals (PhCs), made by periodic distribution of dielectric material with a lattice constant comparable to the wavelength of light, have proved to be powerful tools for efficient control of light propagation [1,2]. A wide range of applications, such as frequency convertors, filters, waveguides, and lasers, can be implemented using PhCs, initiating thus a new approach to photonic circuits, that is, densely integrated devices with multiple optical functionalities [3–6].

Active two-dimensional (2D) PhCs are also interesting candidates for enhancing nonlinear effects due to tight light confinement. In particular, devices for second harmonic generation (SHG) have been investigated in the last years as possible new integrated frequency convertors. It has been demonstrated that one-dimensional and 2D PhCs are ideal materials for nonlinear processes because their unique properties allow simultaneously phase matching and optical field enhancement, two important requirements for efficient SHG [7–12]. However, there appear several problems to be taken into account in order to design an integrated SH-generator photonic device, apart from a stringent requirement of technological precision in the fabrication of the structure. In particular, very small devices require extremely narrow input beams. Working with narrow beams implies confronting mechanisms limiting the efficiency of the SHG: the first one is diffraction—as narrow beams spread over a short propagation distance, their peak intensity decreases. The second one is the phase mismatch, since a narrow beam has a broad distribution in the **k**-vector space, and simultaneously phase matching (PM) all of these spatial Fourier components is difficult. In addition, the out-of-plane losses at both fundamental and SH frequencies decrease the efficiency of the nonlinear process. Finally, one must have a good overlap between the waveguide modes and the in-plane 2D PhC Bloch modes. Simultaneous optimization of all these conditions is a formidable challenge in the design of a PhC nonlinear device.

It has been shown that the use of nondiffractive (or self-collimation) regimes in 2D PhCs may significantly improve the conditions for SHG. It is also known that the diffraction of optical beams can be reduced and even completely suppressed for beams propagating along certain directions in linear PhCs [12–15]. More recently it has been suggested that second-order nonlinear coupling of narrow beams can be substantially enhanced in PhCs tuned to self-collimation regimes [16,17] and, in particular, that an extranarrow beam at the fundamental frequency can be converted into an extranarrow beam at the SH frequency in a 2D PhC [18]. Three simultaneous conditions have to be fulfilled for the efficient conversion: nondiffractive propagation for both fundamental and SH beams, PM condition for maximally broad spatial spectra of both interacting waves, and sufficiently strong nonlinear coupling between the considered Bloch modes. However, in [18] the broad angular range PM is reached for an ideal 2D PhC structure, where the dispersion of the material is neglected.

The introduction of the dispersion of material and the planar configuration results in changes of the dispersive properties of the PhC structure, which are treated in the present article. Therefore, our goal is to design a realistic device where all the previously listed necessary conditions are simultaneously fulfilled. We study a 2D PhC membrane of a highly nonlinear semiconductor material (AlGaAs) and we optimize it through 2D and 3D numerical simulations. In addition, we show that no out-of-plane losses are expected for the input or the SH generated beams. Finally, a 2D nonlinear FDTD numerical study of the optimized structure demonstrates backward SHG and allows the evaluation of the efficiency of the process.

II. DESCRIPTION AND LINEAR OPTIMIZATION OF THE PHOTONIC CRYSTAL

We consider a 2D PhC consisting of a rhombic lattice of air holes etched in a $Al_{0.3}Ga_{0.7}$ As membrane surrounded by air, as schematically represented in Fig. 1(a). We consider a TE-polarized fundamental wave (FW) with a wavelength

*cristian.nistor@upc.edu

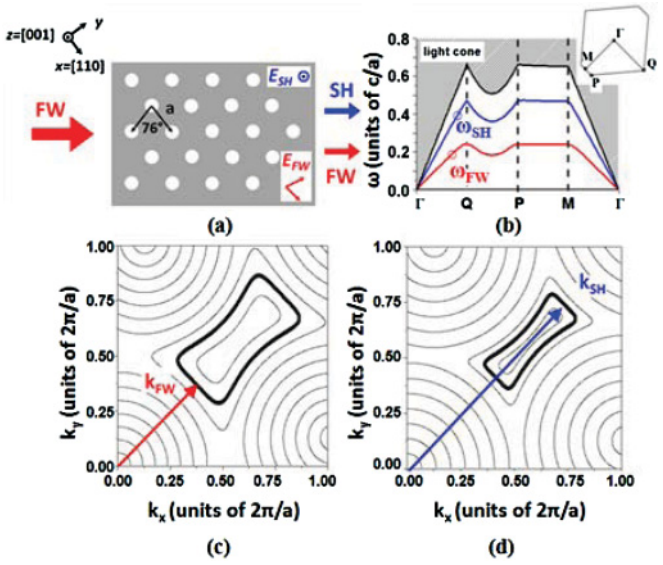

FIG. 1. (Color online) (a) Schematic representation of the 2D PhC. (b) Photonic band diagram for the two chosen modes; the red (lower) line corresponds to the first band for the TE_0 guided mode and the blue (upper) line corresponds to the first band for the TM_2 mode. (c) Isofrequency lines corresponding to the first band for the TE_0 mode. (d) Isofrequency lines corresponding to the first band for the TM_2 mode.

around $\lambda_F = 1.55\ \mu$m, propagating in the [110] direction. A TM-polarized SH beam is generated around $\lambda_{SH} = 0.775\ \mu$m. We consider a nonlinear coefficient $d_{eff} = 97$ pm/V [19]. The refractive indices of $Al_{0.3}Ga_{0.7}As$ at the fundamental and SH wavelength are $n_F = 3.224$ and $n_{SH} = 3.452$, respectively. We have developed a rigorous optimization of the structure parameters in order to fulfill simultaneously the conditions necessary for an efficient SHG using very narrow beams in 2D PhC, as described previously. The optimization was made in a first approximation, considering separately the FW and SH field propagation in a linear 2D structure ($d_{eff} = 0$) with the same effective refractive indices as those of the selected modes of the waveguide. The results were checked by 3D calculations which confirmed the self-collimation regimes at the phase-matched frequencies and the sufficiently large coupling coefficient between the two interacting modes.

The parameters which were varied and analyzed are the thickness of the membrane (with the concomitant effective refractive indices), the diameter of the holes, and the lattice geometry. Also, different combinations of TE and TM modes were explored. After a systematic study using these parameters, we obtained a structure where the optimal thickness for the air/$Al_{0.3}Ga_{0.7}As$/air membrane waveguide for confining the fields in the vertical plane is 350 nm. The wave guide is monomode (TE_0) for the fundamental field at 1.55 μm, with an effective refractive index of the mode $n_F^{eff} = 2.85$. For the SH (0.775 μm) the waveguide is multimode and we chose the TM_2 guided mode with an effective refractive index $n_{SH}^{eff} = 1.425$; the angle of the 2D PhC rhombic lattice is 76°, the lattice constant $a = 322.4$ nm with the hole radius $r = 80.6$ nm, as schematically illustrated Fig. 1(a).

We calculate the band structure of the 2D PhC with these parameters applying the standard technique of plane-wave expansion [20]. The two calculated bands of interest are represented in Fig. 1(b): the FW frequency falls in the first band corresponding to the TE_0 polarized guided mode, represented by the red (lower) line, and the SH frequency in the first band corresponding to the TM_2 polarized guided mode, represented by the blue (upper) line. Note that both bands are placed completely below the light cone, represented by gray area in Fig. 1(b). For the PhC structures proposed in the literature for SHG the fundamental frequency can be placed below the light cone, but the SH usually falls above. Then the generated SH beam couples to the radiative modes in air and consequently suffers vertical losses. The optimization of our particular 2D PhC geometry leads to zero coupling of both FW and SH beams to the radiative modes of the air, a situation that completely eliminates losses for both beams. The vanishing of out-of-plane losses was reported in [21], but in conditions of diffraction similar to those obtained in homogeneous materials for both FW and SH waves, the coupling between the two modes was rather small. In the present article we report a configuration where the out-of-plane losses vanish while there are obtained simultaneous self-collimation regimes for both waves.

The nondiffractive propagation for FW and SH beams is indicated by the dispersion surfaces of the two waves. The optimization of the structure brought us to the situation where the fundamental hits zero diffraction point (the flat segment in the isofrequency lines) in the first TE band and the SH in the first TM band for the propagation direction along the short diagonal of the rhombic structure (ΓQ), as seen in Figs. 1(c) and 1(d), respectively. We identify zero diffraction point for the FW at $\omega_{FW} = 0.208$ (c/a units) and for the SH at $\omega_{SH} = 0.416$ (c/a units), marked with red and blue arrows, respectively, in Figs. 1(c) and 1(d). These frequencies are also marked in the band structure [Fig. 1(b)] with red and blue small circles, respectively. Note that the position of these frequencies on the isofrequency lines indicates that the fundamental field would propagate forward, but the SH would propagate backward [22]. Backward SH generation in PhC was described in [23], where the authors report an increasing of conversion efficiency due to the slow light propagation regime. However, in the present article we follow the self-collimation of FW and backward-generated SH wave, propagation regimes that are checked using 2D FDTD calculations.

For efficient SHG, the FW and SH wave also have to fulfill the PM condition. In Fig. 2 are represented the dispersion curve

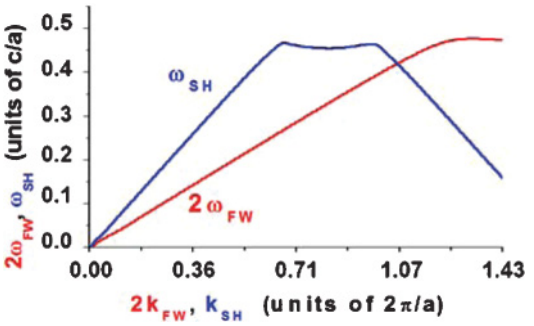

FIG. 2. (Color online) Dispersion curve for the SH (blue line) and the "doubled" dispersion curve for the FW (red line) corresponding to the structure with the parameters described in text.

for the SH wave with a blue (ω_{SH}) line and the "doubled" dispersion curve for the FW (the double of the ω_{FW} versus the double of the modulus of the wave number) with a red ($2\omega_{FW}$) line. The crossing point of the two curves indicates the PM condition and we note that the phase-matched frequencies and wave vectors correspond to nondiffractive propagation regimes.

The last condition that has to be fulfilled by our structure is the nonlinear parametric coupling between the FW and SH modes. A general formalism for a reciprocity theorem and perturbation theory in PhC waveguides was developed in [24,25]. The strength of the nonlinear interaction is characterized by the Hamiltonian of nonlinear interaction which, for parametric processes, can be calculated from the relation

$$H_{\text{int}} = \int d^3r\, P_{\omega}^{(-)} E_{\omega}^{(+)} + \text{H.c.},$$

where $P_{\omega}^{(-)}$ is the polarization and $E_{\omega}^{(\pm)}$ is the scalar part of the electric field operator oscillating as $e^{\mp i\omega t}$. For the case of AlGaAs, which has only one nonvanishing term in the nonlinear susceptibility tensor, the polarization can be written as

$$P_{\omega}^{(-)} = \varepsilon_0 \chi E_{2\omega}^{(-)} E_{\omega}^{(+)} = \varepsilon_0 \chi \varepsilon_{2\omega} \varepsilon_{\omega} E_{2\omega} E_{\omega}^{*} e^{i(k_{2\omega}-k_{\omega})} e^{-i\omega t},$$

with χ the relevant nonlinear susceptibility tensor element. After the integration, at PM ($k_{2\omega} = 2k_{\omega}$) we obtain the following expression for the density of Hamiltonian of interaction:

$$H_{\text{int}} \propto i\left(E_1^2 E_2^{*} + E_1^{*2} E_2\right).$$

Here E_1 and E_2 are the spatial envelopes of the Bloch modes of the FW and SH, respectively. Therefore, in order to evaluate the efficiency of nonlinear coupling, we calculate the cross-correlation between the functions E_1^2 and E_2 normalized in such a way that unity would correspond to the perfect matching of the modes (the interaction of plane waves gives unity under this normalization),

$$K = \frac{\left|\int_M \left(E_1^2 E_2^{*}\right) d\vec{r}\,\right|}{\left(\left|\int_C |E_1^4| d\vec{r}\,\right| \left|\int_C |E_2|^2 d\vec{r}\,\right|\right)^{1/2}},$$

where the upper integral is calculated in the nonlinear material from one unit cell, while the lower integrals are taken over the entire unit cell. We calculated first the coupling coefficient in 2D, representing the 2D overlap of the Bloch modes and we obtained the value $K_B \approx 0.37$. Due to different vertical distribution of the two fields, as they belong to different guided modes, the overlap of the TE_0 mode and the TM_2 mode is $K_W \approx 0.41$. The full 3D overlap results in $K \approx 0.15$.

The results obtained through the linear optimization of our sample presented in this section demonstrate that the $Al_{0.3}Ga_{0.7}As$ PhC membrane with the parameters determined above fulfils the necessary conditions for an efficient nondiffractive SHG. The parameters of the AlGaAs waveguide (as effective refractive indices and dispersion), as well as the periodic structure of air holes, can be achieved from the technological point of view.

III. NONLINEAR FDTD NUMERICAL SIMULATION AND RESULTS

Next, we proceed with nonlinear FDTD simulations in order to analyze the SHG process, check whether the predicted PM condition occurs, and calculate the overall efficiency. The nonlinear FDTD method that we used is described in Ref. [11]. The structure 14 μm wide and 54 μm long is chosen. It is considered and simulated, in the following section, in 2D. From the band structure calculations, we see that the modes propagating at the frequencies in which we are interested, ω and 2ω, fall below the air light line, which renders them, in theory, lossless (in the absence of disorder), justifying that the FDTD calculations can be carried out in 2D.

We first simulate the system by launching a short pulse at ω (centered at 1550 nm, with bandwidth of 150 nm corresponding to a pulse duration of approximately 23 fs) into the structure in order to obtain the intensity of the second harmonic field generated as a function of the wavelength. The modulus of the field amplitude spatial profiles at ω (E_y) and 2ω (E_z) are plotted in Figs. 3(a) and 3(b), respectively, for different time steps. As the FW propagates from left to the right, its spatial distribution on a small scale experiences the periodic nature of the rhombic PhC. The short pulses broaden weakly in propagation due to their nonzero spectral width and obtain a characteristic spatiotemporal shape for the nondiffractively propagating pulses studied in [26]. The SH is generated on the position of the FW pulse and, when the time increases, the SH beam spreads along the structure as it is generated in the opposite direction with respect to the FW propagation direction. In the bottom-most frames of Fig. 3 the FW has already left the structure at the right-hand boundary of the structure, whereas the SH is still in the structure and propagates toward its left border. We can note that the SH beam is highly collimated and does not diffract.

Figure 4 shows the spectrum of the SH generated in the backward direction normalized to the incident FW power (at the centered wavelength of 1550 nm). A sharp peak is obtained at 766 nm very close to the wavelength of the expected PM.

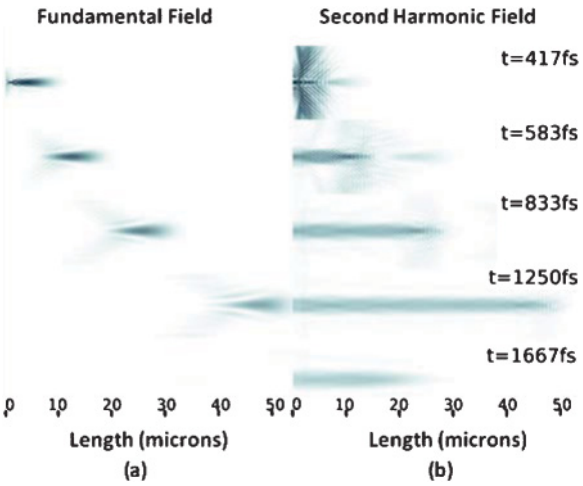

FIG. 3. (Color online) Spatial distribution of the FW (E_y) (left) and the SH (E_z) (right) fields at time steps during the propagation; the modulus of the field abs(E) is represented.

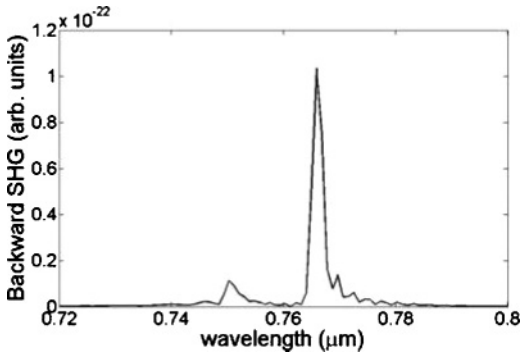

FIG. 4. Spectrum of the SH wave generated in the backward direction normalized to the incident FW.

Next, we simulate the system in the continuous wave regime. The wavelength of the FW is set at 1532 nm, which is double the wavelength of the peak obtained in the pulsed regime, represented in Fig. 4. The spatial distributions of the FW and SH are plotted in Fig. 5 after a sufficiently long time so that the stationary regime is reached.

The high degree of collimation of the FW and the SH is clearly demonstrated in the figures, as the Rayleigh length calculated in homogeneous material for the FW and SH beams are approximately 5 μm for a beamwidth of 2 μm. The field amplitude cross sections are plotted in Figs. 6(a) and 6(b). We also note that the amplitude of the FW is almost constant as it propagates in the structure, except for the first 10 μm. This is an additional proof of the nondiffractive propagation regime at the FW frequency. The SH beam profile shows an almost linear growth with distance in the backward direction, which indicates that the FW and SH are in PM.

The spatial distribution of the FW and SH fields from Fig. 5 were Fourier transformed to obtain the distributions in the wave vector space. The results are shown in Figs. 7(a) and 7(b). We find that the FW is distributed in the k-space according to what is expected from the band structure simulations. The distribution is indeed localized in the first Brillouin zone at a k_x value equal to $\pm 0.64 \times 2\pi/a_x$, where $a_x = 2a \sin(76^\circ/2)$, the other components being the higher-order Bloch harmonics. Around each of these values, the wave-vector distribution spreads vertically in the k_y direction, which indicates that the

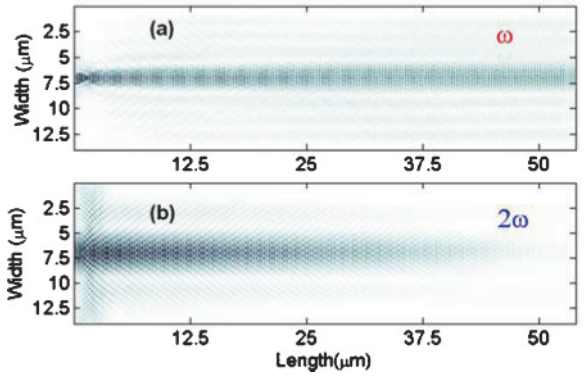

FIG. 5. (Color online) Spatial distribution of the FW (a) (E_y) and the SH (b) (E_z) fields at the time step 2780 fs; the modulus of the field abs(E) is represented.

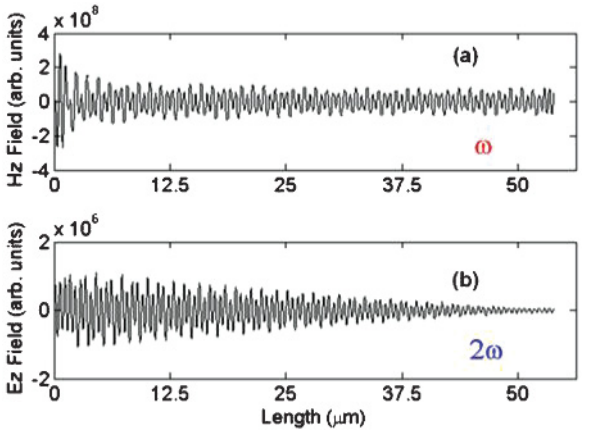

FIG. 6. (Color online) Field cross section at $y = 7$ μm of the FW (a) (E_y) and SHF (b) (E_z).

field propagates in the real space along the x direction with a very low diffraction. At the SH frequency, the field is generated with a specific value of k_x equal to $\pm 0.72 \times 2\pi/a_x$ plus the higher-order Bloch harmonics. Like the FW, the distribution is flat along the k_y direction, indicating the collimation in the real space. The "flat" range of k_y is smaller at the SH frequency than at the FW one, as can be predicted from Fig. 1, representing also the reason why the generated SH beam is broader than the FW beam (in Figs. 3 and 5). The calculations demonstrate that the PM is obtained between the two components indicated by red circles on the figures with wave vector matching given by $k_{2\omega} = 2k_\omega - 2 \times 2\pi/a_x$.

With an input power of 1 GW/cm^2, we obtain a conversion efficiency of 6.3×10^{-4} for the 2D calculations. To calculate the conversion efficiency of the real structure, one must consider the overlap of the TE_0 and TM_2 modes, which is $K_W = 0.41$. As the conversion depends on the square of the overlap coefficient, this results in a conversion of approximately 1.06×10^{-4} for the real 3D structure.

For comparison, we calculate the conversion efficiency in an ideal homogeneous material with the same nonlinear coefficient at the PM condition. We obtain for the nonlinear length (the distance after which the conversion should be 1) the value 6.11×10^{-4} m, which means that after 54 μm

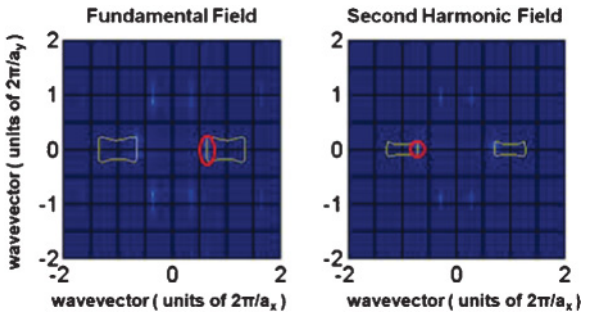

FIG. 7. (Color online) Wave-vector distribution of the FW and the SH fields. The distance used for the wave-vector units are defined by $a_x = 2a \sin(76^\circ/2)$ and $a_y = 2a \cos(76^\circ/2)$ and the red circles indicate the components which are phase matched. We overlay for comparison the equifrequency contours from Fig. 1 in yellow.

(the distance used in the FDTD simulations) the conversion efficiency should be 7.8×10^{-3}. Taking into account the overlap of the two guided modes in the planar structure, the conversion obtained in homogeneous material for the interaction of the TE_0 and TM_2 modes becomes 1.3×10^{-3}. Therefore, the conversion efficiency in PC is lower than in homogeneous materials by a factor of approximately 12, caused mainly by the overlap of the Bloch modes for the two waves in PhC (where it is $K_B = 0.37$, as calculated in Sec. II) compared to the homogeneous case.

IV. CONCLUSIONS

In conclusion, we have suggested and proved the design of a 2D PhC structure with realistic material parameters capable of generating second harmonics using very narrow fundamental beams with diameters comparable to the wavelength of the light. We obtain the characteristics and evaluate the efficiency of the frequency conversion by a full nonlinear FDTD study. The SHG occurs in the backward propagation direction and both fundamental and SH beams propagate under the light cone (without radiative losses) and in a nondiffractive regime. The very good confinement attesting the very low diffractive losses of the fields as well as the estimated SHG efficiency of the process in a very short propagation distance make the structure suitable for applications as frequency convertor in photonic circuits.

ACKNOWLEDGMENTS

This work has been supported by the Spanish Ministerio de Educación y Ciencia through the projects FIS2008-06024-C02-02 and Acciónes Integradas HF 2008-0017 (bilateral collaboration with France)/ PICASSO, by the CRED program of Generalitat de Catalunya, and by the COST action MP0702 from the European Community.

[1] E. Yablonovitch, Phys. Rev. Lett. **58**, 2059 (1987).
[2] S. John, Phys. Rev. Lett. **58**, 2486 (1987).
[3] C. Soukoulis, *Photonic Crystals and Light Localization in the 21st Century* (Kluwer Academic, Dordrecht, The Netherlands, 2001).
[4] C. Husko, A. De Rossi, S. Combrie, Q. V. Tran, F. Raineri, and C. W. Wong, Appl. Phys. Lett. **94**, 021111 (2009).
[5] T. Euser, A. Molenaar, J. Fleming, B. Gralak, A. Polman, and W. Vos, Phys. Rev. B **77**, 115214 (2008).
[6] F. Raineri, C. Cojocaru, R. Raj, P. Monnier, A. Levenson, C. Seassal, X. Letartre, and P. Viktorovitch, Opt. Lett. **30**, 64 (2005).
[7] J. Trull, R. Vilaseca, J. Martorell, and R. Corbalan, Opt. Lett. **20**, 1746 (1995).
[8] M. Scalora, M. J. Bloemer, A. S. Manka, J. P. Dowling, C. M. Bowden, R. Viswanathan, and J. W. Haus, Phys. Rev. A **56**, 3166 (1997).
[9] M. Centini, C. Sibilia, M. Scalora, G. D'Aguanno, M. Bertolotti, M. J. Bloemer, C. M. Bowden, and I. Nefedov, Phys. Rev. E **60**, 4891 (1999).
[10] Y. Dumeige, I. Sagnes, P. Monnier, P. Vidakovic, I. Abram, C. Meriadec, and A. Levenson, Phys. Rev. Lett. **89**, 043901 (2002).
[11] Y. Dumeige, F. Raineri, X. Letartre, and A. Levenson, Electron. Lett. **38**, 1704 (2002).
[12] K. Rivoire, Z. Lin, F. Hatami, W. Ted Masselink, and J. Vuckovic, Opt. Express **17**, 22609 (2009).
[13] D. N. Chigrin, S. Enoch, C. M. Sotomayor Torres, and G. Tayeb, Opt. Express **11**, 1203 (2003).
[14] R. Iliew, C. Etrich, U. Peschel, F. Lederer, M. Augustin, H.-J. Fuchs, D. Schelle, E.-B. Kley, S. Nolte, and A. Tünnermann, Appl. Phys. Lett. **85**, 5854 (2004).
[15] D. W. Prather, S. Y. Shi, D. M. Pustai, C. H. Chen, S. Venkataraman, A. Sharkawy, G. J. Schneider, and J. Murakowski, Opt. Lett. **29**, 50 (2004).
[16] K. Staliunas and R. Herrero, Phys. Rev. E **73**, 016601 (2006).
[17] K. Staliunas, Y. Loiko, R. Herrero, C. Cojocaru, and J. Trull, Opt. Lett. **32**, 1992 (2007).
[18] C. Nistor, C. Cojocaru, Y. Loiko, J. Trull, R. Herrero, and K. Staliunas, Phys. Rev. A **78**, 053818 (2008).
[19] I. Shoji, T. Kondo, A. Kitamoto, M. Shirane, and R. Ito, J. Opt. Soc. Am. B **14**, 2268 (1997).
[20] S. Johnson and J. Joannopoulos, Opt. Express **8**, 173 (2001).
[21] C. Nistor, C. Cojocaru, Y. Loiko, J Trull, and K. Staliunas, J. Opt. A **11**, 114016 (2009).
[22] E. Centeno, D. Felbacq, and D. Cassagne, Phys. Rev. Lett. **98**, 263903 (2007).
[23] R. Iliew, C. Etrich, T. Pertsch, F. Lederer, and Y. S. Kivshar, Phys. Rev. A **81**, 023820 (2010).
[24] D. Michaelis, U. Peschel, C. Wachter, and A. Brauer, Phys. Rev. E **68**, 065601(R) (2003).
[25] G. Lecamp, J. P. Hugonin, and P. Lalanne, Opt. Express **15**, 11042 (2007).
[26] K. Staliunas, C. Serrat, R. Herrero, C. Cojocaru, and J. Trull, Phys. Rev. E **74**, 016605 (2006).